ACS Sustainable Chemistry & Engineering

pubs.acs.org/journal/ascecg

Research Article

Tunable Gas Permeation Behavior in Self-Standing Cellulose Nanocrystal-Based Membranes

Esther E. Jaekel, Steven Kluge, Steffen Tröger-Müller, Murat Tutuş, and Svitlana Filonenko*

Cite This: *ACS Sustainable Chem. Eng.* 2022, 10, 12895−12905

Read Online

ACCESS | Metrics & More | Article Recommendations | Supporting Information

ABSTRACT: Biopolymers arise as environmentally benign alternatives to bio-accumulating, fossil resource-based synthetic polymers for a variety of applications, many of which require self-standing films or membranes. Novel sustainable amine-functionalized cellulose nanocrystals (CNCs) form dense films with low porosity suitable for gas barriers. Due to their brittleness, pure CNC membranes are challenging to work with but represent an attractive support material for selectivity-inducing additives. Supported ionic liquid membranes (SILMs) are promising due to their tunable properties and good performance in gas separation. In this study, we investigate the possibilities to realize such applications by applying glucose and ionic liquids (ILs) as additives with different functions in CNC-based membranes. By the choice of the plasticizer, the gas permeation behavior of the flexible self-standing films can be tuned from impermeable, using glucose as an additive, to permeable by addition of the ILs 1,3-dibutylimidazolium acetate and 1,3-ditetrahydrofurfurylimidazolium acetate. Tunability is also observed through the choice of the CNC source in the form of an inversed selectivity of the gas pair N_2/O_2, which was traceable to the CNCs' source-specific properties. The contributions of the matrix and additive were analyzed by comparing CNC to chitosan membranes and considering gas solubilities and diffusivities. The obtained results underline the diversity and tunability of bio-derived functional materials.

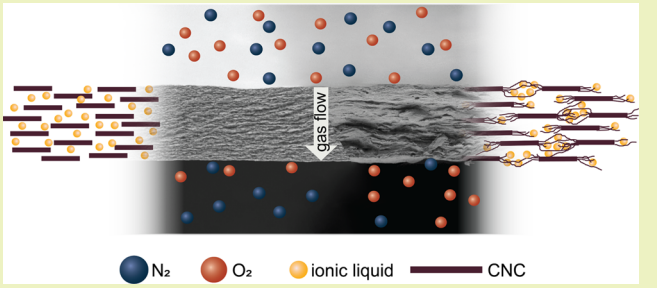

KEYWORDS: *nanocellulose, membranes, sustainable polymers, ionic liquids, supported ionic liquid membranes*

Downloaded via MPI KOLLOID- GRENZFLAECHENFORSCHUNG on September 26, 2022 at 07:57:26 (UTC).
See https://pubs.acs.org/sharingguidelines for options on how to legitimately share published articles.

INTRODUCTION

Polymeric films find applications in a variety of fields, from low-end packaging materials to high-end gas separation membranes. For the creation of a climate-friendly industry, a change of path from using synthetic, bio-accumulating plastics to naturally benign biopolymers is desirable. In the pursuit of reducing non-degradable plastic waste as well as conserving dwindling fossil resources, the most abundant biopolymer cellulose is gaining increasing attention in material science. Due to strong intermolecular hydrogen bonding, processing cellulose in its native form by solubilization is not trivial. Instead, cellulose has been made soluble by tedious derivatization processes in the past, requiring either harmful chemicals (e.g., rayon or cellophane[1]) or changing the native structure to a polymer with decreased biodegradability (e.g., cellulose acetate[2]).

An alternative way of processing cellulose is to break the fiber down into sustainable organic nanomaterials or nanocellulose. Besides cellulose nanofibers fabricated by mechanical fibrillation[3,4] or TEMPO oxidation,[5] cellulose fibers can also be processed into smaller, highly crystalline organic nanoparticles. The cellulose nanocrystals (CNCs) are the building blocks of plant cell walls and thus not only are an abundantly available material but also possess great mechanical strength, which makes them attractive reinforcing additives in material science (examples are provided in Ref.,[6] reviewed in Ref 7.−89). Pure crystalline nanocellulose has also been discovered as an excellent barrier material and has been proven to decrease gas permeability in polymer blends.[10−13] This is due to restricted chain movement in polymer crystallites: gas transfer (or permeance) through non-porous materials follows a solution-diffusion mechanism. Gases can only diffuse in dynamic systems with a transient free volume available to gas molecules to perform Brownian motion.[14] Consequentially, the permeability of polymeric materials usually decreases with an increasing degree of crystallinity.[15] Gases can be separated by permeation through a polymer membrane due to differences in their solubility and diffusivity.

Practical applications as gas barriers or membranes usually require a self-standing film of that polymer. However, the application of CNCs as freestanding films is limited due to

Received: August 10, 2022
Revised: September 2, 2022
Published: September 16, 2022

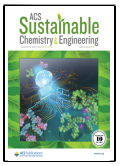

© 2022 The Authors. Published by American Chemical Society

their inherent brittleness, rendering the use of a plasticizer or a matrix material necessary. CNC/polymer composites[16,17] have been studied extensively in the past, revealing improved air barriers and decreased water vapor permeabilities through the use of CNCs as fillers (gluten/CNC composite[18]). CNC films plasticized by small natural molecules, among them several sugar alcohols, have been studied recently, finding flexibility and workability improved by the plasticizer, along with good barrier properties.[19] However, CNCs are much less explored than their sister class cellulose nanofibers (CNFs) since the latter produce more flexible and mechanically stable films. A CNF film plasticized by the ionic liquid (IL) 1-ethyl-3methylimidazolium acetate showed excellent CO_2 selectivities and good permeability at the same time, illustrating the potential of such blends.[20] The possibility to obtain a self-standing and robust membrane even of the rigid CNCs in combination with an IL was demonstrated by Danyliv et al., who used such a membrane as a fuel cell polymer electrolyte.[21] To the best of our knowledge, gas permeation studies have not been conducted on CNC/IL blends.

We recently introduced a new sustainable extraction method that yields CNCs functionalized with amino groups,[22] a functionality that is intrinsic to the biopolymer chitosan, which makes those CNCs more readily biodegradable compared to the standardly used sulfate group-bearing CNCs. Furthermore, amino groups are often exploited for the carbon dioxide adsorbing capabilities.[23,24] We were therefore interested in assessing our new material for a selective effect. Moreover, this study aims to investigate the possibility of tailoring the gas permeation behavior from a gas-tight barrier to a permeable membrane by the choice of the plasticizer. We chose the cellulose monomer glucose as a plasticizer for a gas barrier membrane and two imidazolium-based ILs, 1,3-dibutylimidazolium acetate (dbi acetate) and 1,3-ditetrahydrofurfurylimidazolium acetate (dthfi acetate), to introduce gas permeability and selectivity. Two types of CNCs with different aspect ratios and residual amorphous phase contents are used, and the influences on workability and permeance are analyzed. The fabricated films are compared to films of chitosan combined with the same additives. Chitosan, or polyglucosamin, was chosen due its chemical similarity to amine-functionalized CNCs and is also known as a gas barrier material.[25] This work will contribute to expanding the applicability of CNC-based membranes.

EXPERIMENTAL METHODS

Materials and Reagents. MERCER Stendal GmbH, Arneburg, Germany, provided a pre-fibrillated, never-dried bleached kraft pulp (64 wt % water) for the synthesis of CNCs. CNCs originating from this source will be referred to as fNC. Commercially available short-fibered cellulose powder (Opitec Handel GmbH, Giebelstadt, Germany, cellulose content 100%) was used as an alternative cellulose source. CNCs originating from this material are referred to as sNC in the following. Chitosan with a deacetylation degree of 75−85% and a molecular weight of 50−190 kDa (based on the viscosity of 1 wt % solution in acetic acid) was obtained from Sigma-Aldrich. Ammonium formate (97%) and glycolic acid (98%) were obtained from Alfa Aeser and used without further purification. D-(+)-glucose was obtained from Carl Roth GmbH, Karlsruhe, Germany.

The IL additives 1,3-dibutylimidazolium acetate (dbi acetate) and 1,3-ditetrahydrofurfurylimidazolium acetate (dthfi acetate), shown in Figure 1, were synthesized according to a modified Debus−Radziszewski mechanism as described by Tröger-Müller et al.[26]

Preparation of CNC Dispersion. Positively surface-charged and amine-functionalized CNCs were extracted according to Jaekel et al.[22]

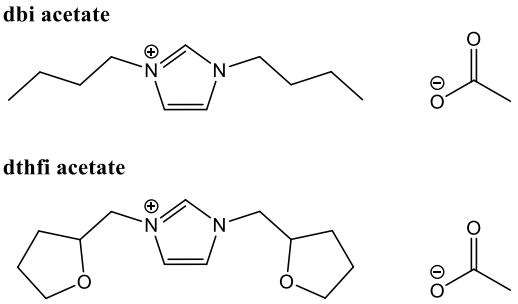

Figure 1. Molecular structure of the used ILs 1,3-di-butylimidazolium acetate (dbi acetate) and 1,3-ditetrahydro-furfurylimidazolium acetate (dthfi acetate).

using different source materials, namely, never-dried fibrillated cellulose (f) and dry short-fiber cellulose (s) as a starting material. Briefly, the starting material (10 wt %) was mixed with the reactive eutectic medium ammonium formate/glycolic acid (molar ratio 2:1). The mixture was reacted in a stirred autoclave at 140 °C for 1 h. The solid residue was separated and washed with centrifugation at 20,000*g* using a sequence of acetic acid (5 vol %) and ethanol until the washing liquid was colorless. The solvent was exchanged with water. The dispersion, including possible precipitates, was homogenized with two passes at a pressure of 1500 bar using an SPCH-EP pressure cell homogenizer (Homogenising Systems Ltd, Stansted, UK). The resulting aqueous CNC dispersion, approximately 10 mg/mL, was diluted to 5 mg/mL before use. Dimensions determined through TEM and the zeta potential of the CNCs and the degree of polymerization (DP) of the CNC-composing cellulose are listed in Table 1. CNCs fabricated from (s) result in higher-aspect ratio CNCs,

Table 1. Properties of Used CNCs[a]

	length [nm]	width [nm]	aspect ratio	zeta potential [mV]	DP
sNC	125 ± 16	6 ± 1	21	35 ±3	215−396
fNC	81 ±14	9 ±1	9	41 ± 3	153−283

[a]Dimensions as determined through TEM; degree of polymerization (DP) refers to the molecular weight of the cellulose chains of dissolved CNCs, determined by GPC.

henceforth denoted sNCs, than CNCs from (f), called fNCs. As indicated in the TEM image in Figure 2 and the size distribution obtained via static light scattering (SLS), longer fibers or aggregates are present in the sNC dispersions, whereas fNCs only consist of nanowhiskers.

Fabrication of CNC-Based Films. The CNC dispersion (5 mg/mL) was mixed with various additives, glucose (glu) or an IL [1,3-dibutylimidazolium acetate (bi) or 1,3-ditetrahydrofurfurylimidazolium acetate (thfi)], in the desired mass ratio. To avoid rapid shrinkage of the drying films, the dispersion's surface tension was decreased by adding 5 vol.% of butanol. The mixture was stirred with a magnetic stirring bar until combined and subsequently sonicated in ice for 15 min to remove air. The dispersion was cast into a PTFE dish (8 cm) and dried in the fume hood at ambient temperature and humidity for 3 days. Masses were chosen to yield dry films with a weight per area of 2 mg cm^{-2}. Resulting films are around 10−13 μm thick. The descriptions and compositions of the produced films are listed in Table S1.

Fabrication of Chitosan-Based Films. Chitosan films with various additives were prepared in a three-step process. First, a casting solution was prepared from chitosan and the additive using a solution of acetic acid in water (1 wt % of acetic acid). Table S2 lists the respective amounts of chitosan and the additive.

The solution was prepared by first weighing the solid compounds into a vial and then adding the solvent in four portions. The vials were closed and stirred using a roller mixer for 3−4 days at 20 rpm. The

https://doi.org/10.1021/acssuschemeng.2c04806
ACS Sustainable Chem. Eng. 2022, 10, 12895−12905

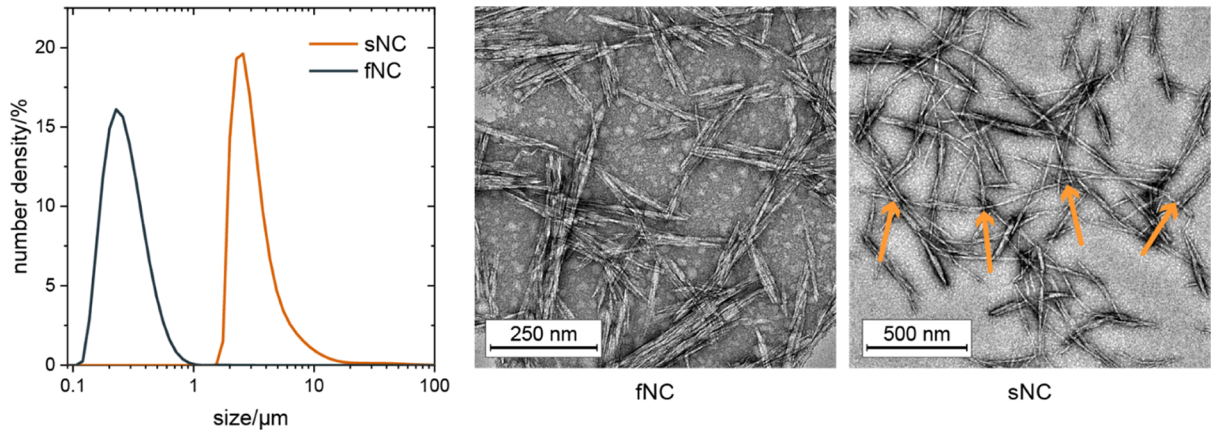

Figure 2. Size distribution as measured with SLS and TEM micrographs of CNCs obtained from pre-fibrillated cellulose (fNC) and short-fiber cellulose (sNC). Orange arrows indicate a fibril observed only in the sNC samples, explaining the larger size observed via SLS.

resulting solutions were clear and highly viscous. In order to remove the air bubbles incorporated during the mixing process, the mixtures were degassed in an ultrasonic bath for up to 2 h. They were then cast on float glass plates using an automated doctor blade (casting speed 17 mm/s; blade height 300 μm). The cast solutions were dried in an ambient atmosphere and at room temperature for at least 6 days.

Gas Permeation Tests. Gas permeation tests were conducted using an EESR time lag apparatus. The measurements were executed at 30 °C with an evacuation duration of 4.5 h after a sample exchange and of 12 time lags (Θ) in between the measurements (minimum 3 min, maximum 6 h). The feed pressure was set to 1000 mbar. The permeate pressure at the beginning of the measurement was adjusted to 1×10^{-4} mbar.

The apparatus measures the time-dependent pressure increase of the permeate so that a time−pressure curve is obtained for every gas. A schematic representation of such a curve is given in Figure S2. From this, two properties can be determined: the permeability P_i and the diffusion coefficient D_i of gas i. The gas permeabilities P_i are calculated according to eq 1

$$P = \frac{l \cdot V(\mathrm{STP})}{A \cdot t \cdot (\Delta p_F - \Delta p_p)} \tag{1}$$

where l is the membrane thickness [cm], V(STP) is the volume of the permeate [cm^3], A is the effective membrane area [cm^2], t is the passed time within the quasi-stationary range [s], Δp_F is the difference of the feed pressure within the quasi-stationary range [cmHg], and ΔpP is the difference of the permeate pressure within the quasi-stationary range [cmHg]. Permeabilities are given in Barrer (1 Barrer $= 10^{-10} \cdot \frac{\mathrm{cm^3(STP) \cdot cm}}{\mathrm{cm^2 \cdot s \cdot cmHg}}$). D_i can be calculated from the time lag Θ according to eq 2

$$D = \frac{l^2}{6\Theta} \tag{2}$$

Θ is determined graphically from the time−pressure diagrams by extrapolating the stationary curve to the time axis.

Solubility can be calculated as the ratio of permeability and diffusivity according to eq 3

$$S = \frac{P}{D} \tag{3}$$

It has no independent significance and is only shown demonstratively.

The films were tested for the permeation of the gases He, H_2, O_2, N_2, CH_4, and CO_2. The membrane ideal selectivity of gas A over gas B was determined by relating the permeabilities of every gas couple according to eq 4

$$\alpha_{A/B} = \frac{P_A}{P_B} \tag{4}$$

Characterization. Scanning electron microscopy (SEM) pictures and electron-dispersive X-ray (EDX) were obtained on a Gemini 1550, Zeiss AG (Oberkochen, Germany) using an accelerating voltage of 2.00 kV or 3.00 kV. Attenuated total reflection infrared (ATR-IR) spectra were measured on a Nicolet iS5 with an iD5 ATR crystal, Thermo Fisher Scientific Inc. (Waltham, Massachusetts, USA), with a resolution of 0,5 cm^{-1}. Size distributions of CNCs were determined using static light scattering (SLS) with a Mastersizer 3000 (Malvern Panalytical, Malvern, UK). Thermogravimetric analysis (TGA) measurements of the membranes were carried out using a thermo-microbalance TG 209 F1 Libra (Netzsch, Selb, Germany) in nitrogen and air atmospheres, with a gas flow of 100 mL min^{-1}. For each measurement, a sample size of 10 ± 1 mg was heated from 25 to 600 °C at a scanning rate of 5 °C min^{-1} in an aluminum crucible. The degradation temperature T_d was defined as the onset temperature of weight loss in the obtained TGA curve. Differential scanning calorimetry (DSC) was performed on a DSC 204 F1 Phoenix (Netzsch, Selb, Germany) using an aluminum crucible with a pierced lid at a heating rate of 5 °C min^{-1}. Data for the thermal analyses were recorded and analyzed using the Proteus (6.1.0) and Quadstar (7.03, MID modus) software packages.

RESULTS AND DISCUSSION

Preparation of CNC Films. Due to their high degree of crystallinity, pure CNC films are very brittle and thus difficult to handle and process. The addition of a plasticizer in the form of smaller molecules may enhance the flexibility of a film. To further promote flexibility, we started producing films with CNCs from a cellulose source that would give a product with a high aspect ratio of 21 and a rather low crystallinity of CrI = 79%, commercially available short-fiber cellulose. CNCs made from this material (sNC) are usually disperse in size (see Figure 2) and contain longer nanofibers with a higher ratio of amorphous domains. Glucose (20% of CNC mass) was added as a small molecule plasticizer. The resulting film, sNC:glu, is semi-transparent and exhibits increased flexibility compared to the pure CNC film (Figure S3). The cross-section observed in SEM reveals a layered structure formed through the horizontally settling rod-shaped particles. It is, however, rather heterogeneous and has a rough surface, likely due to the polydispersity of the CNCs, which can be problematic for reproducible material properties.

Since pure CNC films do not have the mechanical characteristics that can match those of the classical polymers

https://doi.org/10.1021/acssuschemeng.2c04806
ACS Sustainable Chem. Eng. 2022, 10, 12895−12905

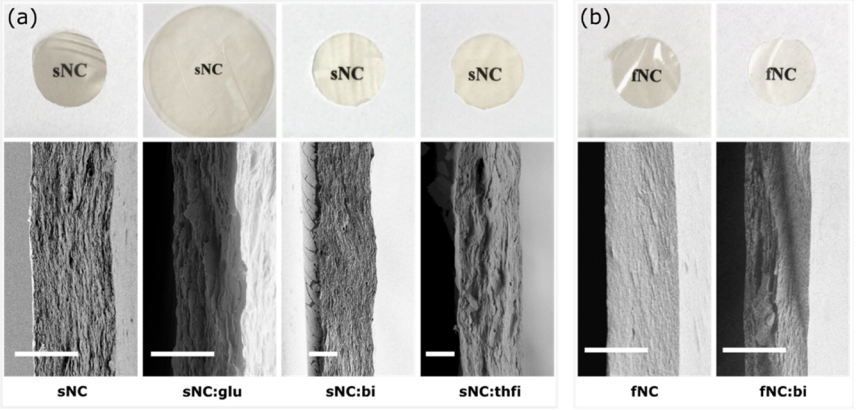

Figure 3. (a,b) Photographs (top row) and SEM cross-section micrographs (bottom row) of the (a) sNC-based and (b) fNC-based films. Scale bar = 10 μm.

suitable for simple applications like packaging, applications with lower mechanical demands are more reasonable. To find out possible applications, we attempted to introduce a plasticizer with inherent functionality into the film. Cellulose is soluble in some imidazolium-based ILs,[27,28] demonstrating a favorable interaction between the two. It is therefore plausible that ILs can be applied as additives in CNC films and they can serve multiple functions in the membranes. Imidazolium-based ILs have been shown to be excellent solvents for CO_2, one of the most climate-harming gases.[29] The idea to exploit this property for the separation of CO_2 from a gas mixture is obvious; however, their liquid state makes application difficult.

Supported ionic liquid membranes (SILMs), in which an IL is immobilized on a solid substrate, shall harness the functionality of an IL while being easy to handle. To this effect, cellulose triacetate membranes doped with imidazolium-based ILs have been used for the separation of the gas couple CO_2/CH_4.[30] Although derived from natural cellulose, the biodegradability of cellulose triacetate is of great concern due to the chemical modification.[31] In this work, we attempted to produce membranes with the two ILs 1,3-dibutylimidazolium acetate (dbi acetate) and 1,3-ditetrahydrofurfurylimidazolium acetate (dthfi acetate) supported by biodegradable CNCs.

The cross-sections of sNC:IL membranes exhibit a layered structure (see Figure 3a), which appears to be interrupted locally by conglomerates. This illustrates a problem arising from the ionic character of the CNC in combination with the addition of an ionic liquid: as a salt, it increases the ionic strength of the casting dispersion and thus causes a decrease of the screening length of the electrostatically stabilized CNC particles. This leads to uncontrolled agglomeration of the CNC, resulting in a heterogeneous film.

In order to obtain a more homogeneous film, CNCs were extracted from a mechanically pre-fibrillated never-dried pulp. As seen in the size distribution measured via SLS (see Figure 2, note the logarithmic scale), CNCs from this cellulose source (fNCs) are smaller on average ($D_x(50)$ = 246 nm vs 2.85 μm) and exhibit a more narrow size distribution. They also have a lower aspect ratio of 9 and a higher crystallinity (85% vs 79%, determined by XRD). Consequentially, the cast film of fNC has a more homogeneous cross-section and a smoother surface, as shown in Figure 3b, but is more brittle.

fNC:bi films are self-standing and flexible enough to be manageable without breaking. The breaking edge of the film observed in SEM (Figure 3b, right), however, illustrates that the film is still brittle. It is more transparent than the sNC films. A self-standing fNC:thfi membrane with equivalent composition could not be obtained as it remained wet after solvent evaporation.

The cross-section of the film appears less heterogeneous than the sNC films, with less conglomerates. This is due to the smaller size distribution and the absence of bigger particles, the agglomeration of which would result in higher disorder. As a result, the film is more densely packed, as illustrated by the significantly lower film thickness despite using the same masses. Moreover, fNCs feature a higher surface charge than sNCs (+41 mV vs +35 mV), which decreases their sensitivity to a change in ionic strength and thus to uncontrolled aggregation. A slight gelling of the casting mixture observed upon addition of the IL, however, demonstrated that solely the slight charge increase is not enough to prevent agglomeration.

fNC films exhibited a tendency to crack during solvent evaporation. Presumably, the high crystallinity, that is, low flexibility, of the film does not facilitate the dispersion of tensions arising throughout the film during drying and consequential shrinking. The amount of IL that can be added while obtaining a self-standing membrane is, however, limited due to the liquid state of this additive at room temperature. The films' tendency to crack during solvent evaporation could not be fully eliminated using this system.

To prevent both cracking and the issue of agglomeration, an amorphous polymer can be added to the casting mixture. Here, xylan, the main component of hemicellulose, was used to sterically stabilize the CNCs. In nature, this polymer has the function of embedding cellulose fibrils in the plant cell wall and therefore also interacts very well with nanocellulose. The addition of xylan (20 wt % in relation to CNC) to the fNC:bi casting mixture visibly decreases the agglomeration and also solves the cracking problem, as illustrated in Figure 6a.

Preparation of Chitosan Films. In contrast to the CNCs, chitosan forms smooth and flexible films even without the use of any additives. The entangled amorphous polymer chains ensure mechanical flexibility and integrity. As shown in Figure 4, the morphology of the chitosan-based films changes as a function of the additives used. The pure film exhibits a disordered and not well-pronounced layered structure with irregular voids. The addition of glucose to the chitosan completely changes the structure of a film to result in a sponge-like material with multiple voids. The addition of dbi acetate reinforces the layered structure. The films using dthfi acetate

https://doi.org/10.1021/acssuschemeng.2c04806
ACS Sustainable Chem. Eng. 2022, 10, 12895−12905

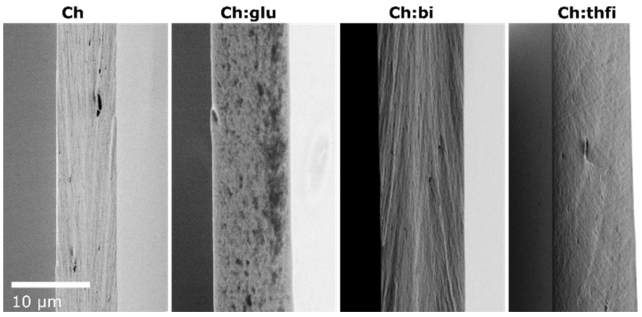

Figure 4. SEM micrographs of the cross-sections of chitosan-based membranes: pure chitosan (CS), chitosan with added glucose (CS:glu), dibutylimidazolium acetate (CS:bi), and ditetrahydrofurfuryl-imidazolium acetate (CS:thfi).

seem to be homogeneous. None of the films possesses percolating pores, which makes them applicable for gas permeation.

Membrane Characterization. After the formation of stable freestanding films, their gas permeation properties were tested. To evaluate the influence of several additives on the gas permeation behavior, two kinds of host polymers were investigated: cellulose nanocrystals, as a highly ordered and crystalline biopolymer colloid with varying crystallinity and length, and chitosan, a soluble biopolymer. Table S3 gives an overview of materials and additives used.

Gas permeation in nonporous membranes is usually assumed to follow the solution-diffusion mechanism.[32] This mechanism separates gases by their molecular properties and their affinity toward the material of the membrane. To aid discussion, Table 2 lists the relevant properties, that is, molecular weight, kinetic diameter, and critical temperature, of the investigated gases.

Table 2. Kinetic Diameter and Critical Temperature of Tested Gases

gas	molecular weight [u]	kinetic diameter[14] [Å]	critical temperature[33] [K]
He	4	2.60	5.2
H_2	2	2.89	32.9
O_2	32	3.46	154.4
N_2	28	3.64	126.1
CH_4	16	3.80	190.6[34]
CO_2	44	3.30	304.2

In the following sections, we discuss the permeation behavior by referring to permeabilities, diffusion coefficients, and solution coefficients of gases in a given membrane. Please note that the applied characterization method determines the permeability and diffusion coefficient from the permeation behavior and calculates the solution coefficient from the obtained data. Hence, the solution coefficients do not provide independent data and are only displayed for visualization.

CNC-Based Membranes. Using two different types of crystalline nanocellulose as the host polymer for different additives, several membranes were produced and their gas permeation behavior was tested. The gas permeabilities are listed in Table S1 and shown in Figure 7a for comparison.

The film composed of sNC and glucose shows an extremely low permeability of around 0.1 Barrer that prohibits to observe any specific selectivity toward the tested gases. The permeability value is close to that of commercial PET (0.09 Barrer) and even several times lower than that of most commonly used biodegradable plastics such as polylactide and poly(γ-butyrolactone) (0.26 and 0.77 Barrer, respectively)[35] despite the use of plasticizer glucose in the sNC film, expected to compromise barrier properties. The sNC:glu film can therefore be considered a barrier material. This result is in accordance with the low gas permeability of disordered (isotropic) CNC films observed previously.[10,11] Multiple studies also showed decreased oxygen permeabilities for CNC-reinforced polymer materials.[12,13] This is attributed to the high crystallinity of CNCs,[22] resulting in little free transient volume in the film. Consequently, the solubilization and/or the mobility of gases is strongly restricted.[15,36] The low gas permeability of CNCs makes them interesting both as an additive and as a main component for applications that require gas tightness, and their biodegradability and biocompatibility are especially attractive and suitable for food-related applications.

To investigate the suitability of CNCs as a matrix or support for a gas-dissolving medium, we exchanged the additive to dbi acetate and dthfi acetate. The anticipated benefit of the IL additives is twofold: on one hand, ILs are known to act as plasticizers for polymers, synthetic[37] as well as natural polysaccharides,[38] and thus increase the permeability of the host material by reducing its crystallinity. On the other hand, they offer the possibility to introduce gas-specific interaction sites such as amines and carbenes, available from imidazolium-based ionic liquids,[39] into the host material. In contrast to the solution-diffusion mechanism, those specific interaction sites increase the affinity of the material toward target gases, thereby changing the membrane's gas selectivity. However, the aspired increase in permeability is in concurrency with selectivity resulting from the plasticizing effect of the IL due to the trade-off between permeability and selectivity, the so-called upper bound as proposed by Robeson.[40,41]

As shown in Figure 5a, the use of both ILs as plasticizers increases the permeability of the films by about 1 order of magnitude compared to glucose. This increase is not as high as expected considering the IL content of 17 wt %. EDX spectra (see Figure S5) reveal a possible reason: spectra collected on the surface of the film have a lower nitrogen content (3.92 wt %) than those collected on the cross-section (10.95 wt %). This retraction of IL into the bulk might be due to the drying in non-polar air, making the interface unattractive for the highly polar IL. Consequentially, the permeability of the surface is lower than that in the bulk, leading to overall lowered values. This issue might be overcome using different drying conditions, such as higher humidity during drying.

While the sNC:glu membrane showed no particular selectivity, that is, almost no differences in the permeabilities of the individual gases, the addition of IL results in a more diverse pattern: the influence on the permeability of individual gases varies, resulting in an increase of the selectivities in individual gas pairs. Ideal selectivities for relevant gas pairs were calculated from the measured data to illustrate those influences, as shown in Table 3. The gas pairs were chosen to reflect different possible applications for the membranes. While this behavior of an increase in both selectivity and permeability despite their mutual tradeoff seems counterintuitive, it is a result of the utter impermeability of sNC:glu.

Comparing the effects of the two ILs used as additives shows that the use of dbi acetate causes a stronger increase in

https://doi.org/10.1021/acssuschemeng.2c04806
ACS Sustainable Chem. Eng. 2022, 10, 12895−12905

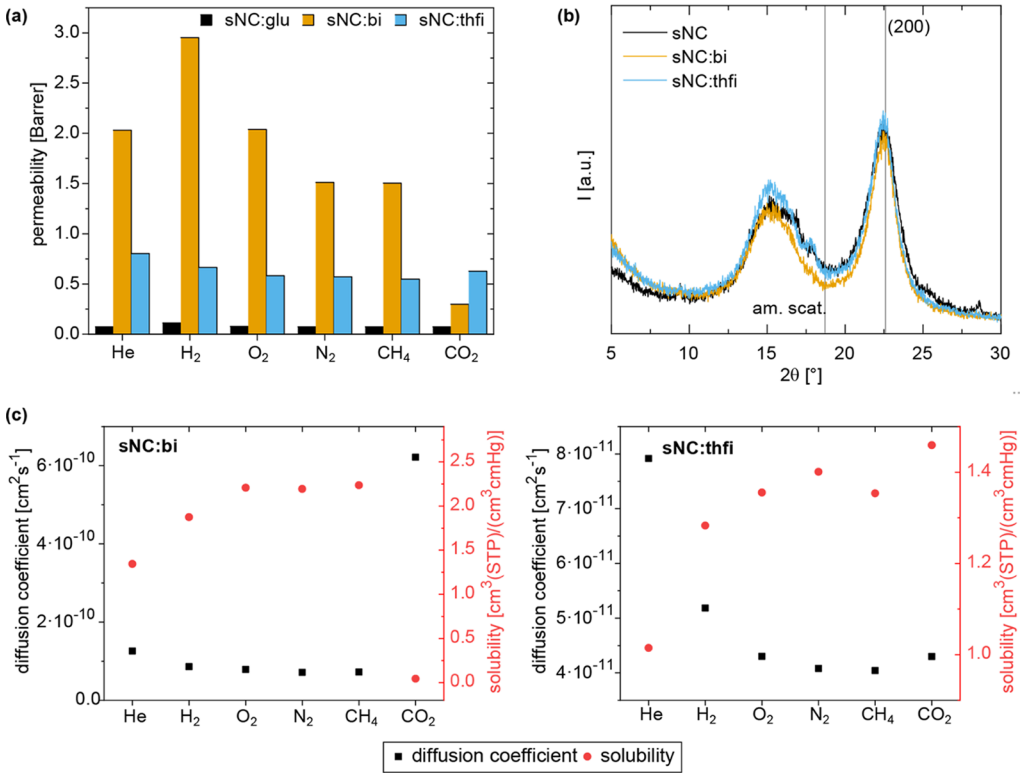

Figure 5. (a) Permeabilities, (b) XRD spectra, and (c) diffusion coefficients and solubilities of selected gases of the sNC-based membranes with the additives glucose (glu), dbi acetate (bi), and dthfi acetate (thfi).

Table 3. Comparison of the Selectivities of the sNC:glu Membrane with the sNC-Based Membranes Containing ILs

	sNC:glu	sNC:thfi	sNC:bi
CO_2/CH_4	0.9	1.0	0.2
He/N_2	1.0	1.3	1.3
H_2/CH_4	1.1	1.6	2.0
O_2/N_2	1.0	1.1	1.4

permeability. This indicates a stronger plasticizing effect of dbi acetate compared to dthfi acetate. We assume that this is a result of the substituents present on the ILs. The flexible butyl chains have more degrees of freedom than the stiff tetrahydrofurfuryl substituents so that the entropy is higher. We therefore estimate the plasticizing effect of the dbi acetate to be more efficient, causing a stronger increase of permeability. XRD analysis (diffractogram shown in Figure 5b) of the films does not show a significant change of crystallinity compared to the pure film. This shows that the ILs are not solvent plasticizers as they do not dissolve crystalline parts but only plasticize the amorphous domains that are already present in the material. For cellulose, the used ILs can therefore be considered nonsolvent or secondary plasticizers.

One peculiarity is found in the permeability of CO_2: its solubility in the measured membranes is in the rather low range of oxygen and nitrogen or even much lower in the case of sNC:bi. The critical temperature of carbon dioxide is 304.2 K, which is the highest among all measured gases. Consequently, the solubility should be higher compared to all the other gases, especially after the inclusion of imidazolium-based ILs with high CO_2 solubility. A high CO_2 permeability would be expected. To investigate the origin of this behavior, we consider the separate contributions of diffusion and solubility. As shown in Figure 5c, the diffusion coefficient of CO_2 is significantly higher than those of the other gases, despite its higher molecular weight. This hints at a facilitated transport of CO_2 compared to the other gases, likely due to a favorable interaction between the membrane and CO_2. The solubility, on the other hand, is low compared to the other gases. It seems like the gas passes the membrane very fast but also saturates the membrane very quickly. This behavior is not observed in the membrane with dthfi acetate, sNC:thfi.

As seen in the SEM images (compare Figure 3a,b), the change of the matrix material sNC to the smaller fNC resulted in a more ordered and more densely packed film. The denser packing should be reflected in a lower gas permeability. As expected, fNC-type membranes indeed exhibit lower permeabilities when comparing films with the same additive (sNC:bi and fNC:bi). The addition of xylan (fNC:X:bi) increases the permeability toward oxygen and nitrogen (see Figure 6) and changes the selectivities in their favor.

In contrast to sNC:bi, fNC:bi does not exhibit the low CO_2 permeability despite using the same IL, which contradicts an attribution of this phenomenon to dbi acetate. Instead, we observe another peculiarity: the selectivity toward the gas pair O_2/N_2. Due to the properties of molecular oxygen and nitrogen, the solution-diffusion mechanism usually allows faster permeation of oxygen and not nitrogen through polymeric membranes.[42] This is due to the smaller kinetic diameter and higher critical temperature of oxygen (the solubility correlates with the critical temperature, see Table 2[43]). However, we observe an O_2/N_2 selectivity of around 0.9. This inversed behavior in the case of the fNC:bi-type membranes hints at another interaction mechanism. An O_2/N_2 selectivity below 1 usually indicates a gas transport that is dominated by pore flow, or more specifically Knudsen

https://doi.org/10.1021/acssuschemeng.2c04806
ACS Sustainable Chem. Eng. 2022, 10, 12895−12905

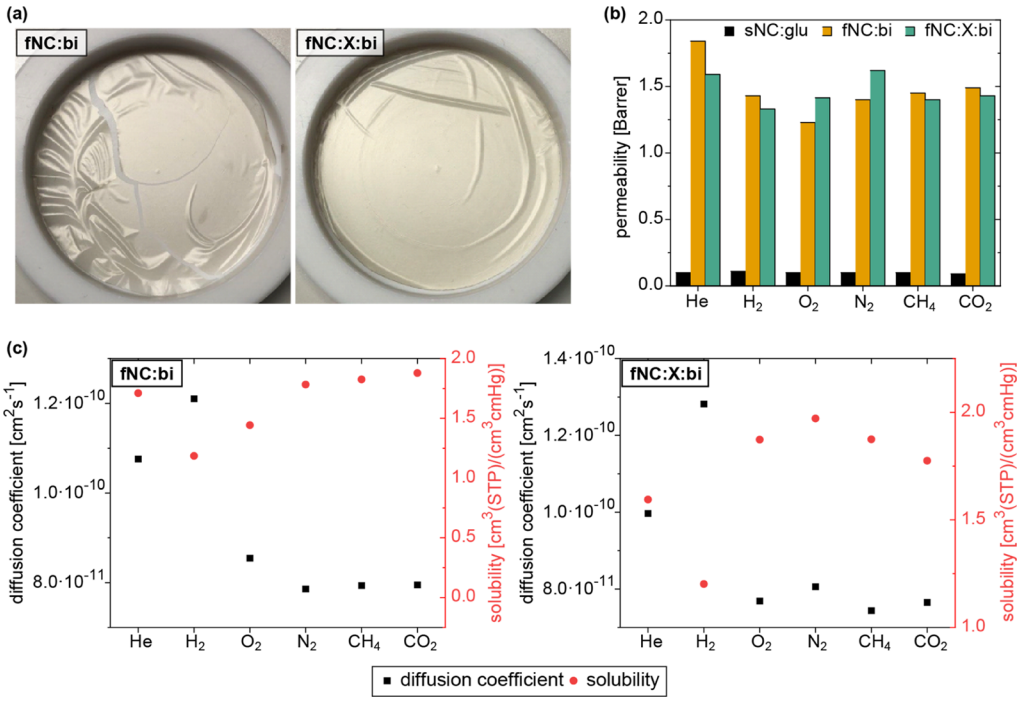

Figure 6. (a) Comparison between the fNC:bi membrane without (left) and with (right) addition of xylan (b) permeabilities of the fNC-based membranes with the additives dbi acetate (bi) and xylan (X) compared to the sNC:glu membrane (c.f. Table 4 for numerical selectivities). (c) Diffusion coefficients and solubilities of selected gases in the membranes fNC:bi and fNC:X:bi.

Table 4. Ideal Selectivities for Selected Gas Pairs in the fNC:bi-type Membranes Compared to sNC:glu[a]

	sNC:glu	fNC:bi 1	fNC:bi 2	fNC:bi 3	fNC:X:bi 1	fNC:X:bi 2
CO_2/CH_4	0.9	0.7	0.5	0.4	1.0	1.1
He/N_2	1.0	1.7	2.1	1.3	1.0	1.0
H_2/CH_4	1.1	1.9	2.3	1.0	1.1	0.8
O_2/N_2	1.0	0.9	0.9	0.9	0.9	0.8

[a]The number represents different samples of the same composition.

diffusion, implying the presence of percolating pores in the membrane which were not visible in the SEM micrographs. The Knudsen diffusion coefficient is correlated with the mean free path length of a gas molecule and is proportional to $M_w^{-1/2}$: the smaller M_w of N_2 compared to O_2 would therefore lead to a slightly higher permeability (Ismail 2015: calculated O_2/N_2: 0.93;[14] Pinnau 1991: 0.91 for defected membranes[44]). The presence of pores would also demand higher permeabilities for the gases with even lower M_w, such as He, H_2, and CH_4. However, the permeability of the significantly lighter H_2, for instance, only lies in the same range as nitrogen and is even lower in the membrane fNC:X:bi, which strongly contradicts the hypothesized pore flow. As shown in Table 4, this peculiar behavior is present over several tests and samples and can as such not be considered a simple measurement error or deviation. It is also unchanged by the addition of xylan.

The separate consideration of diffusion coefficient and solubility are depicted exemplary for fNC:bi 3 in Figure 6c. The measured diffusivity value is slightly higher for O_2 than for N_2. Consequentially, the higher permeability (the product of diffusion coefficient and solubility) of N_2 appears to originate from a higher solubility, reflected in the displayed values. In membrane fNC:X:bi, both the diffusion coefficient and solubility were measured to be higher for N_2.

Chitosan-Based Membranes. In order to investigate the origin of the peculiar gas permeation behavior in the amino group containing CNC-based membranes, the influence of IL addition on the permeation behavior was investigated in chitosan-based membranes. Membranes were prepared using the same mass ratios of polymer to plasticizer. Unlike CNCs, chitosan forms highly amorphous membranes: XRD spectra of the dried CS films show broad amorphous scattering instead of the sharp diffraction peaks of the (020) plane at 10° and the (110) plane at 20° for all the films.

The permeation results are shown in Figure 7a. Pure chitosan is known to have a low gas permeability so that the measured permeabilities are expectedly low. In contrast to the CNC-based membranes, the chitosan-based membranes do not generally show increased permeability upon additive addition. In fact, glucose and dbi acetate even lower the permeability of the membrane for almost all gases and are therefore no plasticizers for the polymer. CO_2 appears to be an exception: its extremely low permeability in pure chitosan might be due to the saturation through carbamate formation between the amino groups and CO_2.[45] Every additive increases CO_2 permeability, possibly due to the disturbance of the carbamate formation through the interaction between the additive and amino group. The addition of dthfi acetate increases the permeability of most gases, with the exception of oxygen and nitrogen, and is therefore a more efficient plasticizer. The selectivities of selected gas pairs are listed in Table 5.

https://doi.org/10.1021/acssuschemeng.2c04806
ACS Sustainable Chem. Eng. 2022, 10, 12895−12905

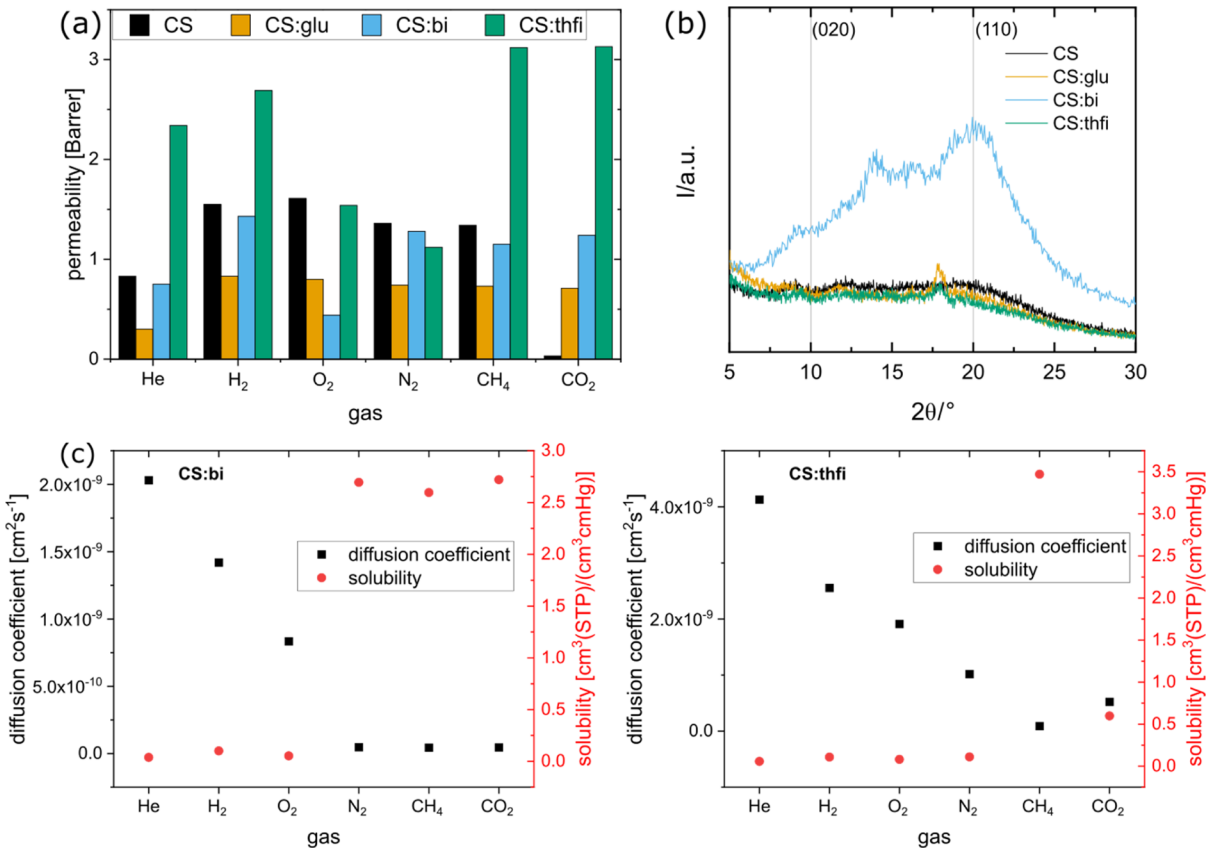

Figure 7. (a) Permeabilities of the chitosan-based membranes CS, CS:glu, CS:bi, and CS:thfi. (b) Diffractograms of the chitosan-based membranes show mostly amorphous scattering, indicating a low degree of crystallinity. (c) Diffusion coefficients and solubilities of selected gases in the membranes CS:bi and sNC:thfi.

Table 5. Comparison of the Selectivities of CS:pure with the CS-Based Membranes Containing ILs

	CS	CS:bi	CS:thfi
CO_2/CH_4	0.02	1.1	1.0
He/N_2	0.6	0.6	2.1
H_2/CH_4	1.2	1.2	0.9
O_2/N_2	1.2	0.3	1.4

Interestingly, we observe the same trend of inversed O_2/N_2 selectivity in the CS:bi membrane as in the fNC analogue. CS:bi exhibits a significantly higher solubility for nitrogen than for oxygen which is not observed in CS:thfi, as shown in Figure 7c. CS:thfi is characterized by a selectively and significantly increased solubility of methane, while the solubilities of the other gases are very low. Transport is accelerated in comparison to the other chitosan membranes mainly by increased diffusion coefficients, proving the plasticizing effect of the IL.

DISCUSSION

Unexpected gas permeation behavior was observed mainly for dbi acetate-containing membranes. To investigate the roles of the IL and the matrix material, we take a closer look at the diffusion coefficient and the solubility separately in relation to their determining molecular properties, kinetic diameter, and critical temperature, respectively, in the following section. The data for all measured gases and membranes are plotted in Figure 8.

sNC membranes appear to be largely dominated by the transport behavior of the matrix itself: this is supported by the predominantly expected relations between diffusion coefficient and kinetic diameter (D decreases with increasing diameter) as well as solubility and critical temperature (S increases with increasing T_c). The addition of the ILs increases mostly the gas solubilities without affecting selectivities or diffusion coefficients much. The ILs seem to plasticize only the amorphous regions of the polymer matrix without being an active agent in gas transport.

An exception of this behavior is CO_2, which has a drastically decreased solubility and an increased diffusion coefficient in the sNC:bi membrane. Since this is not observed in any other dbi acetate-containing membrane, it seems unlikely that this behavior is traceable to the IL. We do see a very low permeability of CO_2, however, in one other membrane: the pure chitosan membrane CS. Just like for sNC:bi, this is attributed to a low CO_2 solubility (see Figure 8). We argued that the low permeability might be due to the presence of amino groups in the chitosan, which immobilize the gas via carbamate formation—the same could be true for the used sNC, which, due to the aminolysis during the extraction process, also bears amino groups. The gas desorption step might then be impeded by a high energy barrier, consequentially leading to a low permeability of CO_2.

An unexpected O_2/N_2 selectivity smaller than 1 was observed only for dbi acetate-containing membranes. Membranes with other or no additives show the expected O_2/N_2 selectivity and comparable solubilities (see Figure S4,

https://doi.org/10.1021/acssuschemeng.2c04806
ACS Sustainable Chem. Eng. 2022, 10, 12895−12905

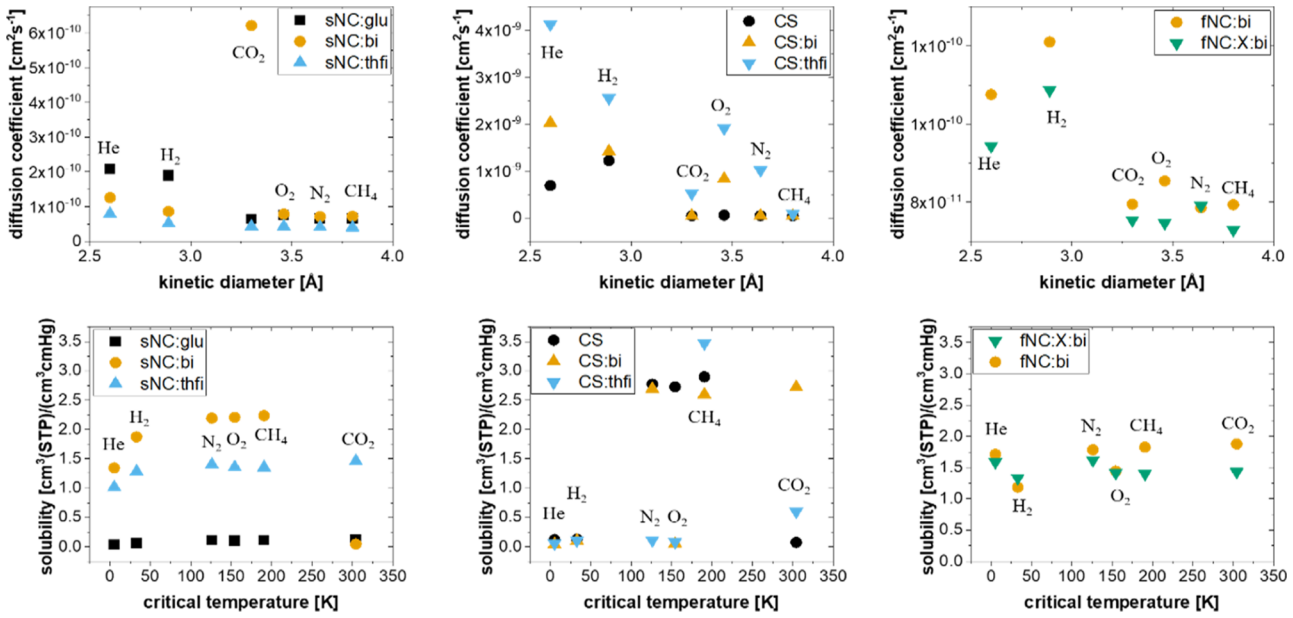

Figure 8. Diffusion coefficients in relation to the kinetic diameter and solubilities in relation to critical temperature of selected gases in the membranes CS:bi and sNC:thfi

Supporting Information). Judging from this, the low O_2/N_2 selectivity seems to be an attribute of the IL instead of the polymer matrix. However, there is one exception: sNC:bi does not show the same behavior, that is, it does not reflect the N_2-solubilizing properties of the IL. This is another indication for the hypothesis that in sNC-type membranes, sNC has a bigger influence on the gas transport than the IL. The cause might lie in the higher ratio of amorphous domains in the sNC membranes, which hypothetically causes a shift in the type of free transient volume available for gas transport: with more amorphous cellulose present, more IL is actually incorporated into the polymer and serves as a plasticizer. The plasticized amorphous cellulose domains determine the gas transport, and the IL does not actively solubilize gases itself as it is consumed for plasticization. In the fNC membranes, on the other hand, the amorphous ratio is much smaller so that gases are transported predominantly through the IL and not through cellulose. This hypothesis is supported by the different permeation of CH_4 in dthfi acetate-containing membranes: in CS:thfi, the solubility of CH_4 is significantly higher than that of the other gases, implying a good solubility in the IL. In sNC:thfi, CH_4 solubility is in the same range as the solubilities of the other gases, indicating that the IL is no active agent in gas transport here.

CONCLUSIONS

Self-standing films based on two types of amine-functionalized CNCs with different crystallinities and sizes and glucose and ILs as additives were tested as gas barrier and gas separation membranes (supported IL membranes). A particular gas selectivity due to amino groups on the CNCs was not observed, confirming the CNCs as a neutral support for selectivity-inducing ILs. CNC membranes plasticized with glucose exhibited excellent gas barrier properties, while CNC membranes with ILs are permeable toward gases with low selectivities. The studied ILs have different effects in the investigated biopolymers, ranging from non-solvent/secondary plasticizer to active gas transport agent, reflected in unexpected gas permeabilities of the membranes. Despite consisting of the same polymer, cellulose, we observed different gas permeation behaviors between the two types of CNCs, sNC and fNC. In particular, an unusual selectivity of the gas pair O_2/N_2 was found in fNC dbi acetate membranes, which was not reflected in sNC dbi acetate membranes. When compared to chitosan-based membranes with equivalent composition, this curious behavior was traced to the IL dbi acetate, which seems to exhibit a high solubility for nitrogen. The dominance of IL or matrix material in gas transport properties seems to shift, depending on the used polymer and its crystallinity index as well as the used IL, which highlights the diversity and tunability of bioderived functional materials. Overall, we suggest that in a matrix with a crystallinity as high as the CNC films, the gas permeation mechanism of the fabricated composite CNC-IL membranes must be considered a function of crystallinity of the applied CNC. Moreover, the IL dbi acetate seems to reverse the typically observed O_2/N_2 permeation behavior, which might open interesting possibilities in gas separation.

ASSOCIATED CONTENT

Supporting Information

The Supporting Information is available free of charge at https://pubs.acs.org/doi/10.1021/acssuschemeng.2c04806.

Additional experimental details; scheme of the experimental setup; and additional characterization data including gas permeabilities, photographs, SEM images, and thermal and FTIR analysis (PDF)

AUTHOR INFORMATION

Corresponding Author

Svitlana Filonenko − *Max Planck Institute of Colloids and Interfaces, 14476 Potsdam, Germany;* orcid.org/0000-0001-6888-877X; Email: svitlana.filonenko@mpikg.mpg.de

https://doi.org/10.1021/acssuschemeng.2c04806
ACS Sustainable Chem. Eng. 2022, 10, 12895−12905

Authors

Esther E. Jaekel − *Max Planck Institute of Colloids and Interfaces, 14476 Potsdam, Germany*

Steven Kluge − *Fraunhofer Institute for Applied Polymer Research, 14476 Potsdam, Germany*

Steffen Tröger-Müller − *Fraunhofer Institute for Applied Polymer Research, 14476 Potsdam, Germany*

Murat Tutuş − *Fraunhofer Institute for Applied Polymer Research, 14476 Potsdam, Germany*

Complete contact information is available at: https://pubs.acs.org/10.1021/acssuschemeng.2c04806

Funding

Open access funded by Max Planck Society.

Notes

The authors declare no competing financial interest.

■ ACKNOWLEDGMENTS

E.E.J. and S.F. gratefully acknowledge Max Planck Society for financial support. S.K., S.T.-M., and M.T. gratefully acknowledge Fraunhofer Society for financial support.

■ REFERENCES

(1) Kauffman, G. B. Rayon: The first semi-synthetic fiber product. *J. Chem. Educ.* **1993**, *70*, 887.

(2) Puls, J.; Wilson, S. A.; Hölter, D. Degradation of Cellulose Acetate-Based Materials: A Review. *J. Polym. Environ.* **2011**, *19*, 152−165.

(3) Chen, W.; et al. Individual cotton cellulose nanofibers: pretreatment and fibrillation technique. *Cellulose* **2014**, *21*, 1517−1528.

(4) Stelte, W.; Sanadi, A. R. Preparation and Characterization of Cellulose Nanofibers from Two Commercial Hardwood and Softwood Pulps. *Ind. Eng. Chem. Res.* **2009**, *48*, 11211−11219.

(5) Saito, T.; Kimura, S.; Nishiyama, Y.; Isogai, A. Cellulose Nanofibers Prepared by TEMPO-Mediated Oxidation of Native Cellulose. *Biomacromolecules* **2007**, *8*, 2485−2491.

(6) Azizi Samir, M. A. S.; Alloin, F.; Sanchez, J.-Y.; Dufresne, A. Cellulose nanocrystals reinforced poly(oxyethylene). *Polymer* **2004**, *45*, 4149−4157.

(7) Dufresne, A. Cellulose nanomaterial reinforced polymer nanocomposites. *Curr. Opin. Colloid Interface Sci.* **2017**, *29*, 1−8.

(8) Mariano, M.; El Kissi, N.; Dufresne, A. Cellulose nanocrystals and related nanocomposites: Review of some properties and challenges. *J. Polym. Sci., Part B: Polym. Phys.* **2014**, *52*, 791−806.

(9) Habibi, Y.; Lucia, L. A.; Rojas, O. J. Cellulose Nanocrystals: Chemistry, Self-Assembly, and Applications. *Chem. Rev.* **2010**, *110*, 3479−3500.

(10) Chowdhury, R. A.; et al. Cellulose Nanocrystal (CNC) Coatings with Controlled Anisotropy as High-Performance Gas Barrier Films. *ACS Appl. Mater. Interfaces* **2019**, *11*, 1376−1383.

(11) Herrera, M. A.; Mathew, A. P.; Oksman, K. Gas permeability and selectivity of cellulose nanocrystals films (layers) deposited by spin coating. *Carbohydr. Polym.* **2014**, *112*, 494−501.

(12) Dhar, P.; Bhardwaj, U.; Kumar, A.; Katiyar, V. Poly (3-hydroxybutyrate)/cellulose nanocrystal films for food packaging applications: Barrier and migration studies. *Polym. Eng. Sci.* **2015**, *55*, 2388−2395.

(13) Nuruddin, M.; et al. Structure-Property Relationship of Cellulose Nanocrystal-Polyvinyl Alcohol Thin Films for High Barrier Coating Applications. *ACS Appl. Mater. Interfaces* **2021**, *13*, 12472−12482.

(14) Ismail, A. F.; Khulbe, K. C.; Matsuura, T. *Gas Separation Membranes: Polymeric and Inorganic*; Ismail, A. F., Chandra Khulbe, K., Matsuura, T., Eds.; Springer International Publishing: Cham, 2015; pp 11−35.

(15) Bitter, J. G. A. Effect of crystallinity and swelling on the permeability and selectivity of polymer membranes. *Desalination* **1984**, *51*, 19−35.

(16) Kargarzadeh, H.; et al. Recent developments on nanocellulose reinforced polymer nanocomposites: A review. *Polymer* **2017**, *132*, 368−393.

(17) Calvino, C.; Macke, N.; Kato, R.; Rowan, S. J. Development, processing and applications of bio-sourced cellulose nanocrystal composites. *Prog. Polym. Sci.* **2020**, *103*, 101221.

(18) Rafieian, F.; Shahedi, M.; Keramat, J.; Simonsen, J. Mechanical, thermal and barrier properties of nano-biocomposite based on gluten and carboxylated cellulose nanocrystals. *Ind. Crops Prod.* **2014**, *53*, 282−288.

(19) Fernández-Santos, J.; Valls, C.; Cusola, O.; Roncero, M. B. Improving Filmogenic and Barrier Properties of Nanocellulose Films by Addition of Biodegradable Plasticizers. *ACS Sustainable Chem. Eng.* **2021**, *9*, 9647−9660.

(20) Janakiram, S.; et al. Humidity-responsive molecular gate-opening mechanism for gas separation in ultraselective nanocellulose/IL hybrid membranes. *Green Chem.* **2020**, *22*, 3546−3557.

(21) Danyliv, O.; Strach, M.; Nechyporchuk, O.; Nypelö, T.; Martinelli, A. Self-Standing, Robust Membranes Made of Cellulose Nanocrystals (CNCs) and a Protic Ionic Liquid: Toward Sustainable Electrolytes for Fuel Cells. *ACS Appl. Energy Mater.* **2021**, *4*, 6474−6485.

(22) Jaekel, E. E.; Sirviö, J. A.; Antonietti, M.; Filonenko, S. One-step method for the preparation of cationic nanocellulose in reactive eutectic media. *Green Chem.* **2021**, *23*, 2317−2323.

(23) Qian, Z.; Wei, L.; Mingyue, W.; Guansheng, Q. Application of amine-modified porous materials for CO2 adsorption in mine confined spaces. *Colloids Surf., A* **2021**, *629*, 127483.

(24) Vilarrasa-García, E.; Cecilia, J. A.; Moura, P. A. S.; Azevedo, D. C. S.; Rodríguez-Castellón, E. Assessing CO2 Adsorption on Amino-Functionalized Mesocellular Foams Synthesized at Different Aging Temperatures. *Front. Chem.* **2020**, *8*, 591766.

(25) Kurek, M.; Šćetar, M.; Voilley, A.; Galić, K.; Debeaufort, F. Barrier properties of chitosan coated polyethylene. *J. Membr. Sci.* **2012**, *403−404*, 162−168.

(26) Tröger-Müller, S.; Brandt, J.; Antonietti, M.; Liedel, C. Green Imidazolium Ionics-From Truly Sustainable Reagents to Highly Functional Ionic Liquids. *Chem.—Eur. J.* **2017**, *23*, 11810−11817.

(27) Fukaya, Y.; Hayashi, K.; Wada, M.; Ohno, H. Cellulose dissolution with polar ionic liquids under mild conditions: required factors for anions. *Green Chem.* **2008**, *10*, 44−46.

(28) Swatloski, R. P.; Spear, S. K.; Holbrey, J. D.; Rogers, R. D. Dissolution of Cellose with Ionic Liquids. *J. Am. Chem. Soc.* **2002**, *124*, 4974−4975.

(29) Wang, S.; Wang, X. Imidazolium Ionic Liquids, Imidazolylidene Heterocyclic Carbenes, and Zeolitic Imidazolate Frameworks for CO2 Capture and Photochemical Reduction. *Angew. Chem., Int. Ed.* **2016**, *55*, 2308−2320.

(30) Lam, L.; et al. Cellulose triacetate doped with ionic liquids for membrane gas separation. *Polymer* **2016**, *89*, 1.

(31) Yadav, N.; Hakkarainen, M. Degradable or not? Cellulose acetate as a model for complicated interplay between structure, environment and degradation. *Chemosphere* **2021**, *265*, 128731.

(32) Javaid, A. Membranes for solubility-based gas separation applications. *Chem. Eng. J.* **2005**, *112*, 219−226.

(33) Haynes, W. M. L.; David, R. *CRC Handbook of Chemistry and Physics*, 101 ed, Internet Version, 2020.

(34) Ambrose, D.; Tsonopoulos, C. Vapor-Liquid Critical Properties of Elements and Compounds. 2. Normal Alkanes. *J. Chem. Eng. Data* **1995**, *40*, 531−546.

(35) Sangroniz, A.; et al. Packaging materials with desired mechanical and barrier properties and full chemical recyclability. *Nat. Commun.* **2019**, *10*, 3559.

(36) Horacek, H. Diffusion, Löslichkeit und Permeation niedrigmolekularer Verbindungen in Polymeren. *Berichte der Bunsengesellschaft für physikalische Chemie* **1979**, *83*, 352−360.

(37) Rahman, M.; Brazel, C. S. Ionic liquids: New generation stable plasticizers for poly(vinyl chloride). *Polym. Degrad. Stab.* **2006**, *91*, 3371−3382.
(38) Sankri, A.; et al. Thermoplastic starch plasticized by an ionic liquid. *Carbohydr. Polym.* **2010**, *82*, 256−263.
(39) Hollóczki, O.; et al. Carbene Formation in Ionic Liquids: Spontaneous, Induced, or Prohibited? *J. Phys. Chem. B* **2013**, *117*, 5898−5907.
(40) Robeson, L. M. Correlation of separation factor versus permeability for polymeric membranes. *J. Membr. Sci.* **1991**, *62*, 165−185.
(41) Robeson, L. M. The upper bound revisited. *J. Membr. Sci.* **2008**, *320*, 390−400.
(42) Kluge, S.; Weiß, M. Herstellung und Charakterisierung von Polysulfon-Membranen für die Gastrennung. *Chem. Ing. Tech.* **2021**, *94*, 585.
(43) De Angelis, M. G.; Sarti, G. C.; Doghieri, F. NELF model prediction of the infinite dilution gas solubility in glassy polymers. *J. Membr. Sci.* **2007**, *289*, 106−122.
(44) Pinnau, I.; Koros, W. J. Structures and gas separation properties of asymmetric polysulfone membranes made by dry, wet, and dry/wet phase inversion. *J. Appl. Polym. Sci.* **1991**, *43*, 1491−1502.
(45) Qaroush, A. K.; et al. Chemisorption of CO2by chitosan oligosaccharide/DMSO: organic carbamato-carbonato bond formation. *Green Chem.* **2017**, *19*, 4305−4314.

https://doi.org/10.1021/acssuschemeng.2c04806
ACS Sustainable Chem. Eng. 2022, 10, 12895−12905